Investigation of electron spin dynamic in the bichromatic Kapitza-Dirac effect via frequency ratio and amplitude of laser beams

Asma Ebadati,[1] Mohsen Vafaee,[2] and Babak Shokri[1,3]

[1]*Laser and Plasma Research Institute, Shahid Beheshti University, G. C., Evin, Tehran, Islamic Republic of Iran*
[2]*Department of Chemistry, Tarbiat Modares University, P.O. Box 14115-175, Tehran, Islamic Republic of Iran*
[3]*Physics Department, Shahid Beheshti University, G. C., Evin, Tehran, Islamic Republic of Iran*

(Received 29 April 2019; published 27 November 2019)

We discuss electron diffraction from two standing waves with two different frequencies. The effects of increasing the frequency of the second laser beam and changing the laser amplitudes on the form and period of the Rabi oscillation are studied theoretically. The corresponding scattering probabilities for certain incident electron momenta are obtained by an analytical Rabi matrix and numerical solution of the Dirac equation. We show that at high intensities, $\geqslant 10^{20}$ W cm^{-2}, the process with an even number of photons involved in the Kapitza-Dirac effect can be used as a spin filter for free electrons. On the other hand, the process with an odd number photons and an electron with momentum along the laser polarization preserves the initial spin of the electron.

DOI: 10.1103/PhysRevA.100.052514

I. INTRODUCTION

Recent developments in high-power lasers raised hopes to polarize electrons and positrons with ultraintense laser fields [1–3] and produce spin-polarized beams for new applications in high-energy physics [4]. There are methods (mechanisms) for efficient electron (positron) polarization, e.g., spin-dependent radiation reactions [5,6], laser wake field acceleration in prepolarized plasmas [7], radiative polarization in a storage ring via the Sokolov-Ternov effect [8,9], and beam splitters [10].

Recently, there have been notable theoretical and experimental studies in the spin polarization of electrons via interferometric beam splitters in high-intensity laser interactions. These studies rely on the diffraction of electrons from the periodic potential generated by laser waves, the Kapitza-Dirac (KD) effect [11]. A relativistic treatment by field intensities in excess of 10^{20} W cm^{-2} and field frequencies in the x-ray range was presented to analyze the spin dynamics of electrons in monochromatic and bichromatic standing waves [12–15]. The recent researches proposed that the KD effect and specific polarization combination of the two laser pulses could control the spin polarization of electron beams [10,16]. The spin properties of the scattered electron beam were discussed in bichromatic standing waves with frequency ratios 1:2 and 1:3 [17,18]. Also new studies show that the energy of subrelativistic electrons can be strongly modulated on the few-femtosecond timescale via an interaction with a high-intensity optical traveling wave created in vacuum by two counterpropagating laser pulses at different frequencies [19,20]. This effect can serve as a generator for the attosecond ballistic bunching of electrons. Furthermore, inelastic scattering of subrelativistic electrons in bichromatic standing waves was studied for three-photon ($\omega : 2\omega$) and four-photon ($\omega : 3\omega$) processes [21].

In the original version, the KD effect can be understood as a combined absorption and emission process involving two photons. The electron absorbs a photon of momentum $\vec{k}$ from one of the laser beams and emits a photon of momentum $-\vec{k}$ into the counterpropagating laser beam. Therefore, the outgoing electron momentum changes by $2\vec{k}$. A similar effect is considered in the case of two counterpropagating waves with different colors, $E_1 \cos(\omega_1 t - k_1 x)$ and $E_2 \cos(\omega_2 t + k_2 x)$. In the Bragg regime and with the energy and momentum conservation laws for the process, the electron absorbs N photons from the one wave and emits L photons to the other wave. Due to the opposite directions of momenta $\mathbf{k_1}$ and $\mathbf{k_2}$ of the two laser fields, the electron momentum changes by $N\mathbf{k_1} - L\mathbf{k_2}$. In previous studies of the two-color Kapitza-Dirac effect, the three-photon KD effect [electron scattering in standing waves composed of two photons with fundamental frequency ($N = 2$) and one photon of its second harmonic ($L = 1$)] and the four-photon KD effect [electron scattering in standing waves composed of three photons with fundamental frequency ($N = 3$) and one photon of its third harmonic ($L = 1$)] were investigated. To study the KD effect involving more photons, we use other higher-order (fourth, fifth, sixth, seventh, and eighth) harmonics as the second laser beam. In the following, we investigate the interference of a fundamental laser beam with higher-order harmonics as counterpropagating waves in the bichromatic KD effect to manipulate and characterize the scattered electron spin. In this case, questions arise: Can the interaction of an unpolarized electron beam with more photons in the Kapitza-Dirac effect be used to spin-polarize the electrons? Does the increase in the number of photons in the KD effect with a higher-order-harmonic beam distinctly change the electron spin dynamics?

In this work, we investigate the spin effects of an electron for the high-number photon KD effect caused by adding a second standing wave with commensurate frequency, i.e., 1:4, 1:5, 1:6, 1:7, and 1:8. Our paper is organized as follows. In Sec. II and the Appendix, we present an analytical treatment which relies on the relativistic Volkov states of the Dirac

TABLE I. The Rabi frequency $\hat{\Omega}$ for various polarization configurations of the bichromatic standing waves with different frequency ratios. The definition $\sigma_\pm = \sigma_x \pm i\sigma_y$ is applied.

Case	$\vec{\epsilon}_1$	$\vec{\epsilon}_2$	$\hat{\Omega}_{\omega:2\omega}$	$\hat{\Omega}_{\omega:3\omega}$	$\hat{\Omega}_{\omega:4\omega}$	$\hat{\Omega}_{\omega:5\omega}$
1	$\vec{e}_x$	$\vec{e}_x$	$\frac{5}{4\hbar}p_x c + \frac{i}{2}\omega\sigma_y$	$-\frac{27i}{8}\frac{p_x\omega}{c}\sigma_y$	$-\frac{i}{2}\omega\sigma_y$	$\frac{625i}{128}\frac{p_x\omega}{c}\sigma_y$
2	$\vec{e}_x$	$\vec{e}_y$	$-\frac{i}{2}\omega\sigma_x$	$\frac{27i}{8}\frac{p_x\omega}{c}\sigma_x - \frac{9i}{16}\omega\sigma_z$	$4i\frac{p_x\omega}{c}\sigma_z + \frac{i}{2}\omega\sigma_x$	$-\frac{625i}{128}\frac{p_x\omega}{c}\sigma_x + \frac{125i}{256}\omega\sigma_z$
3	$\vec{e}_y$	$\vec{e}_x$	$\frac{1}{4\hbar}p_x c + \frac{i}{2}\omega\sigma_y$	$\frac{9i}{16}\omega\sigma_z$	$-\frac{i}{2}\omega\sigma_y$	$-\frac{125i}{256}\omega\sigma_z$
4	$\vec{e}_y$	$\vec{e}_y$	$-\frac{i}{2}\omega\sigma_x$	0	$\frac{i}{2}\omega\sigma_x$	0
5	$\frac{1}{\sqrt{2}}(\vec{e}_x + i\vec{e}_y)$	$\frac{1}{\sqrt{2}}(\vec{e}_x + i\vec{e}_y)$	$\frac{1}{\sqrt{2}\hbar}p_x c$	0	0	0
6	$\frac{1}{\sqrt{2}}(\vec{e}_x + i\vec{e}_y)$	$\frac{1}{\sqrt{2}}(\vec{e}_x - i\vec{e}_y)$	0	0	0	0
7	$\frac{1}{\sqrt{2}}(\vec{e}_x - i\vec{e}_y)$	$\frac{1}{\sqrt{2}}(\vec{e}_x - i\vec{e}_y)$	$\frac{5}{4\sqrt{2}\hbar}p_x c + \frac{1}{2\sqrt{2}}\omega\sigma_+$	$-\frac{27}{16}\frac{p_x\omega}{c}\sigma_+ + \frac{9}{16}\omega\sigma_z$	$-\frac{4}{\sqrt{2}}\frac{p_x\omega}{c}\sigma_z - \frac{1}{2\sqrt{2}}\omega\sigma_+$	$\frac{625}{256}\frac{p_x\omega}{c}\sigma_+ - \frac{125}{256}\omega\sigma_z$
8	$\frac{1}{\sqrt{2}}(\vec{e}_x + i\vec{e}_y)$	$\vec{e}_x$	$\frac{1}{2\hbar}p_x c$	0	0	0
9	$\frac{1}{\sqrt{2}}(\vec{e}_x - i\vec{e}_y)$	$\vec{e}_x$	$\frac{3}{4\hbar}p_x c + \frac{i}{2}\omega\sigma_y$	$-\frac{27i}{8\sqrt{2}}\frac{p_x\omega}{c}\sigma_y + \frac{9}{16\sqrt{2}}\omega\sigma_z$	$-2\frac{p_x\omega}{c}\sigma_z - \frac{i}{2}\omega\sigma_y$	$\frac{625i}{128\sqrt{2}}\frac{p_x\omega}{c}\sigma_y - \frac{625i}{256\sqrt{2}}\omega\sigma_z$
10	$\vec{e}_x$	$\frac{1}{\sqrt{2}}(\vec{e}_x + i\vec{e}_y)$	$\frac{5}{4\sqrt{2}\hbar}p_x c - \frac{1}{2\sqrt{2}}\omega\sigma_-$	$\frac{27}{8\sqrt{2}}\frac{p_x\omega}{c}\sigma_- - \frac{9}{16\sqrt{2}}\omega\sigma_z$	$\frac{4}{\sqrt{2}}\frac{p_x\omega}{c}\sigma_z + \frac{1}{2\sqrt{2}}\omega\sigma_-$	$-\frac{625}{128\sqrt{2}}\frac{p_x\omega}{c}\sigma_- + \frac{125}{256\sqrt{2}}\omega\sigma_z$
11	$\vec{e}_x$	$\frac{1}{\sqrt{2}}(\vec{e}_x - i\vec{e}_y)$	$\frac{5}{4\sqrt{2}\hbar}p_x c + \frac{1}{2\sqrt{2}}\omega\sigma_+$	$-\frac{27}{8\sqrt{2}}\frac{p_x\omega}{c}\sigma_+ + \frac{9}{16\sqrt{2}}\omega\sigma_z$	$-\frac{4}{\sqrt{2}}\frac{p_x\omega}{c}\sigma_z - \frac{1}{2\sqrt{2}}\omega\sigma_+$	$\frac{625}{128\sqrt{2}}\frac{p_x\omega}{c}\sigma_+ - \frac{125}{256\sqrt{2}}\omega\sigma_z$

equation. Our numerical results are presented in Sec. III. First, we show the time evolution of an electron in the counterpropagating bichromatic laser waves with various harmonics. Then we discuss the dependence of the results on the frequency ratios of the standing waves. We finish with some comparative conclusions about even and odd numbers of photons involved in the KD effect.

II. SPIN-DEPENDENT STIMULATED COMPTON SCATTERING

The Kapitza-Dirac effect can be regarded as stimulated Compton scattering. We therefore start from the S matrix for multiphoton Compton scattering:

$$S = \frac{ie}{c}\int d^4x\, \bar{\psi}_{p',s'} \not{A}_2 \psi_{p,s}. \tag{1}$$

Here,

$$\psi_{p,s}(x) = \sqrt{\frac{mc}{Vp^0}}\left(1 - \frac{e\not{k}_1\not{A}_1(k_1x)}{2ck_1p}\right)u_{p,s}e^{-ipx+i\Lambda_p}, \tag{2}$$

with

$$\Lambda_p = \frac{1}{ck_1p}\int^{k_1x}\left[ep\mathcal{A}_1(\phi) + \frac{e^2}{2c}\mathcal{A}_1^2(\phi)\right]d\phi, \tag{3}$$

represents the Dirac-Volkov state for the incoming electron dressed by the field A_1^μ and counterpropagating field A_2^μ [22–24]. Accordingly, $\psi_{p',s'}$ is the Dirac-Volkov state for the scattered electron, c is the speed of light, m is the electron rest mass, and V is a normalization volume. The free Dirac spinors $u_{p,s}$ are spin polarized along the z axis. We employ the Feynman slash notation $\not{A} = \gamma A = \gamma^\mu A_\mu$ for scalar products of four-vectors with the Dirac matrices γ^μ. Moreover, throughout this paper we set $\hbar$, the reduced Planck constant, to unity for convenience.

In the following we derive the Rabi frequency for the five-photon bichromatic ($\omega : 4\omega$) and six-photon bichromatic ($\omega : 5\omega$) processes. The Appendix provides the derivation details of the Rabi frequency for five- and six-photon processes. By neglecting the terms with higher order of p_x, we derive the effective term of the Rabi frequency of order m^{-1} in the five-photon KD effect as

$$\hat{\Omega}_{\omega:4\omega} = +\frac{i}{2}\omega\vec{\epsilon}_1{}^4(\vec{\epsilon}_2^* \times \vec{e}_z)\cdot\vec{\sigma} + 4i\frac{p_x}{c}\omega(\vec{\epsilon}_1\cdot\vec{e}_x)\vec{\epsilon}_1{}^2(\vec{\epsilon}_1\times\vec{\epsilon}_2^*)\cdot\vec{\sigma}, \tag{4}$$

and for the six-photon KD effect as

$$\hat{\Omega}_{\omega:5\omega} = +\frac{125i}{256}\omega\vec{\epsilon}_1{}^4(\vec{\epsilon}_1\times\vec{\epsilon}_2^*)\cdot\vec{\sigma} - \frac{625i}{128}\frac{p_x}{c}\omega(\vec{\epsilon}_1\cdot\vec{e}_x)\vec{\epsilon}_1{}^4(\vec{\epsilon}_2^*\times\vec{e}_z)\cdot\vec{\sigma}. \tag{5}$$

The Rabi frequency is indicated for polarization combination of the fundamental frequency laser beam with its second, third, fourth, and fifth harmonic separately in Table I. Following the results of the analytical method [17,18], here we can emphasize some interesting points of this table. First of all, the existence of $\sigma_\pm$ in the Rabi matrix is a sign of spin dependency of the Rabi oscillation. That means if this term is the only term of the Rabi matrix, the electron can be spin polarized by the KD effect. Second, the σ_z term in the Rabi matrix has no effect on the spin polarization of the electron along the x or y directions.

III. NUMERICAL RESULTS AND DISCUSSION

In order to evaluate our analytical predictions, we have implemented numerical simulations. The Dirac equation

$$\left(i\not{\partial} + \frac{e}{c}\not{A}(x) - mc\right)\psi(x) = 0 \tag{6}$$

was solved in the presence of the bichromatic vector potential $A(x) = A_1(k_1x) + A_2(k_2x)$. Here $A_1(kx)$ is the fundamental laser beam and $A_2(nkx)$ represents its nth harmonic, in this work the fourth, fifth, sixth, seventh, or eighth harmonic. We model the temporal interaction of the electron with the laser beam in these numerical simulations with a trapezoidal shape and comprise ten cycles of the fundamental laser period for turn-on and turn-off [18]. We transform the Dirac equation (6) into momentum space using an expansion of the electron

wave function over the momentum eigenstates of the form

$$\psi(x) = \sqrt{\frac{k}{2\pi}} \sum_n \sum_\zeta c_n^\zeta(t) u_n^\zeta e^{ip_n x}. \tag{7}$$

The coefficients c_n^ζ $(n = 0, \pm1, \pm2, \ldots)$ are related to the states with $p_n = (p_x, 0, nk)$ momentum. Also the bispinors u_n^ζ are defined as

$$u_n^{+\uparrow/+\downarrow} = \sqrt{\frac{\varepsilon_n + mc^2}{2\varepsilon_n}} \begin{pmatrix} \chi^{\uparrow/\downarrow} \\ \frac{nck\hbar\sigma_x}{\varepsilon_n + mc^2} \chi^{\uparrow/\downarrow} \end{pmatrix},$$
$$u_n^{-\uparrow/-\downarrow} = \sqrt{\frac{\varepsilon_n + mc^2}{2\varepsilon_n}} \begin{pmatrix} -\frac{nck\hbar\sigma_x}{\varepsilon_n + mc^2} \chi^{\uparrow/\downarrow} \\ \chi^{\uparrow/\downarrow} \end{pmatrix}, \tag{8}$$

with $\chi^\uparrow = (1, 0)^\top$ and $\chi^\downarrow = (0, 1)^\top$ and the relativistic energy momentum relation $\varepsilon_n = \sqrt{(mc^2)^2 + c^2 p_n^2}$. The index $\zeta \in \{+\uparrow, +\downarrow, -\uparrow, -\downarrow\}$ labels the sign of the energy and the spin direction. These states can be denoted by $|nk, \zeta\rangle$. Inserting this ansatz into the Dirac equation and employing a Crank-Nicolson scheme yields coupled ordinary differential equations for time-dependent expansion coefficients. In the numerical simulation, however, these systems are truncated to a finite number of momentum modes, $-n_{\max} < n < n_{\max}$, with $n_{\max}$ large enough for convergence. Therefore, the occupation probabilities as a function of the interaction time are obtained.

The specific setup of two counterpropagating waves with frequency ratio $1 : n$ $(n = 4, 5, 6, 7, 8)$ is encoded by the vector potential

$$\vec{A}_{(\omega:n\omega)} = A_1[\cos(kz)\cos(kct)\vec{\epsilon}_1] + A_2[\cos(nkz)\cos(nkct)\vec{\epsilon}_2], \tag{9}$$

where A_1 and A_2 are the amplitudes of standing waves and ϵ_1 and ϵ_2 are polarization vectors. Taking into account the practical feasibility, the parameters of the available high-intensity light sources with field frequencies in the x-ray range, such as the European XFEL (Hamburg) and LCLS (Stanford) [25], have been chosen for the numerical simulation. In the following numerical calculation, for each multiphoton KD effect, the electron is considered with appropriate initial momentum and its mirror state. The electron with initial longitudinal momentum (momentum component in the direction of the laser propagation) of $p_z = -4k$ in the presence of a five-photon bichromatic $(\omega : 4\omega)$ vector potential corresponds to the scattered state with $p_z = +4k$. Similarly, the electron in the six-photon bichromatic $(\omega : 5\omega)$ vector potential is elastically scattered, with its longitudinal momentum reverted from $p_z = -5k$ to $p_z = +5k$.

A. Linear-linear polarization laser beams in multiphoton KD effect

We take a closer look at the simplest asymmetric setup for two linearly polarized counterpropagating laser waves with frequency ratio $1 : n$. At the same time, we choose the electron momentum to be perpendicular to the direction of both laser waves. Our numeric result indicates that, for each scattering, the same form of Rabi oscillation would arise. The shape of the oscillation, similar to the result of bichromatic

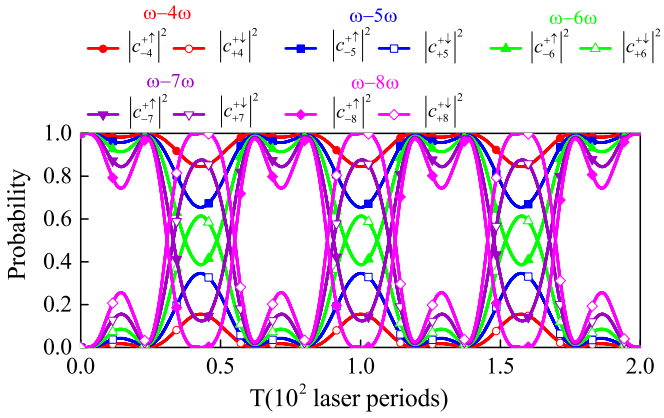

FIG. 1. Temporal evolution of the occupation probability in five-, six-, seven-, eight-, and nine-photon KD effects with linear fundamental beam and counterpropagating linear high-order-harmonic laser beam. The vector potential that we used in this simulation is $\vec{A} = A_1 \cos(kz)\cos(\omega t)\vec{e}_x + A_2 \cos(nkz)\cos(n\omega t)\vec{e}_x$. The laser parameters are $\lambda = 0.6$ nm for wavelength, $eA_1 = 2n \times 10^4$ eV for amplitude of the fundamental laser beam, and $eA_2 = 2 \times 10^4$ eV for amplitude of the high-order-harmonic laser beam. The initial electron momentum along the laser propagation for each scattering is under the Bragg condition and has no component on the polarization plane.

$(\omega : 3\omega)$ standing waves via a selective vector potential with $\cos(\omega_{1,2}t)$ part, is sinusoidal and has two distinct peaks [18]. As the previous results have pointed out, there is an additional term in the vector potential that causes this change in Rabi oscillation form. If the constant vector potential is used in the simulation, the same spin dynamic is observed with a typical Rabi oscillation. Due to higher harmonic orders for the counterpropagating wave, the overall intensity and the amplitude of oscillation increase. As an illustration, the occupation probability of initial and scattered modes for each multiphoton KD effect is depicted in Fig. 1. The form of the Rabi oscillation even with increasing frequency ratio in bichromatic standing waves is unchanged.

In Fig. 2 all multiphoton KD effects have equal overall intensity. In this case the amplitude of high-order harmonics is chosen to $A_2 = A_1/n$, and because of decreasing intensity, the amplitude of oscillation is reduced. The form and period of the Rabi oscillation are unchanged. It should be noted that, in all reviewed bichromatic standing waves for linearly polarized laser beams, the spin dynamics of the electron shows spin flipping. The symmetry of spin flipping exists and the same kind of Rabi oscillation would arise if the electron was incident with opposite spin state. According to the numerical results, another interesting point to note here is that the frequency of the Rabi oscillation in each multiphoton scattering does not change with changing laser amplitudes in a scattering. For instance, the Rabi oscillations in Figs. 1 and 2 with blue (square symbol) lines for six-photon KD scattering, even with different laser amplitudes, have the same frequency. Due to the vector potential we described for bichromatic standing waves, the Rabi frequency of the n-photon KD effect scales with $\cos(\omega t)^n(\frac{ea_1}{mc^2})^n \cos(n\omega t)(\frac{ea_2}{mc^2})$ and with changing $a_{1,2}$ (respectively the fundamental and high-order-harmonic laser amplitudes) the final Rabi frequency remains constant.

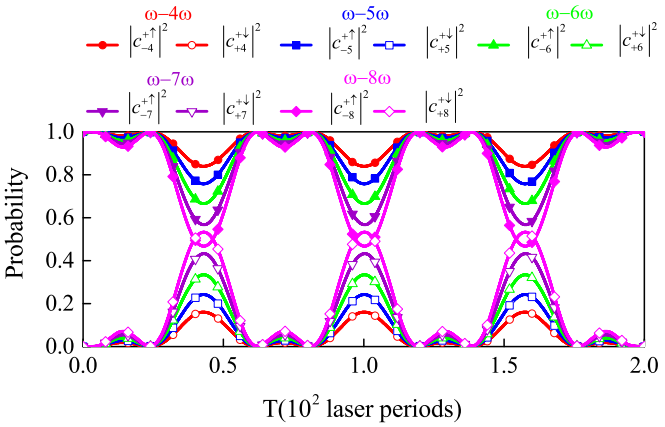

FIG. 2. Temporal evolution of the occupation probability in five-, six-, seven-, eight-, and nine-photon KD effects with linear fundamental beam and counterpropagating linear high-order-harmonic beam with $\vec{A} = A_1 \cos(kz)\cos(\omega t)\vec{e}_x + A_2 \cos(nkz)\cos(n\omega t)\vec{e}_x$ as the vector potential. The wavelength of the laser is $\lambda = 0.6$ nm. By choosing $eA_1 = 2 \times 10^4$ eV for the fundamental laser beam and $eA_2 = A_1/n$ eV for the nth harmonic laser beam in each scattering, the combined intensity for all scattering is equal. The initial electron momentum along the laser propagation for each scattering is under the Bragg condition and has no component on the polarization plane.

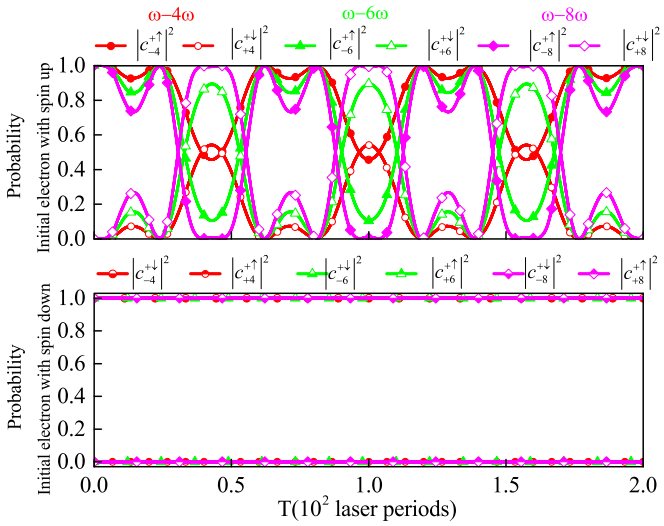

FIG. 3. Temporal evolution of the occupation probability of an initial electron with spin up (upper panel) and initial electron with spin down (lower panel) in five-, seven-, and nine-photon KD effects with a linearly polarized fundamental beam and circularly polarized harmonic laser beam. The numeric results are obtained with $\vec{A} = A_1 \cos(kz)\cos(\omega t)\vec{e}_x + \frac{A_2}{\sqrt{2}}\cos(nkz)\cos(n\omega t)\vec{e}_x - \frac{A_2}{\sqrt{2}}\sin(nkz)\cos(n\omega t)\vec{e}_y$ as the vector potential. The wavelength of the laser is $\lambda = 0.6$ nm. The amplitude of the high-order-harmonic laser beam is $eA_2 = 2 \times 10^4$ eV and, to obtain equal overall intensity in these three processes, we select eA_1 properly. The electron enters the laser field with momentum along the laser field direction. For a spin-down electron in five-, seven-, and nine-photon KD effects, no scattering takes place.

In a forthcoming study we intend to investigate the effect of vector potential variation on Rabi oscillation frequency due to the laser amplitude changes.

B. Combination of linear and circular polarization of laser beams in multiphoton KD effect

Recent progress in the theory shows that significant polarization for electrons can be acquired in a circularly polarized standing laser wave. This spin separation via setup with the circular polarization of a high-order-harmonic and linear fundamental laser beam were observed in the three- and four-photon KD effect [6,17,18]. In this research we investigate the numerical solution for the same setup of polarization in other multiphoton KD effects with higher-order harmonics. We start with the five-photon KD effect and provide the details of analytical and numerical results.

In the case of the circular polarization for the high-frequency laser beam in the five-photon KD effect, for instance, cases 10 and 11 of Table I, it can be predicted that the Rabi oscillation is spin dependent. The diffraction probability resulting from numerical simulation for a combination of the fourth harmonic with circular polarization and the linear polarized fundamental laser beam (case 10) is plotted with red (circle symbol) lines in Fig. 3. The electrons are scattered only when they are initially in the spin-up state and spin-down electrons will remain in their initial state. By replaying left-handed circular polarization for the fourth harmonic (case 11), only the initial spin-down electrons are transferred to the spin-flipping state and the spin-up electrons do not diffract. This property can be used to separate spin-up from spin-down electrons as a spin-filter device. The Rabi oscillations with $|-4, +\downarrow\rangle$, $|+4, +\uparrow\rangle$, and $|+4, +\downarrow\rangle$ states appear for an incident electron state $|-4, +\uparrow\rangle$ with nonzero transverse momentum in the linearly polarized fundamental laser beam and circularly polarized fourth harmonic. As expected for cases 10 and 11 of Table I, for nonvanishing values of p_x, the Rabi matrix contains an additional spin-independent term.

Interestingly, numeric results confirm the similar spin dynamics for the electron with the same setup polarization in the seven- and nine-photon KD effects. As is presented in Fig. 3, by proper selection of laser beam amplitudes with identical overall intensity for the bichromatic standing waves with frequency ratios 1:4, 1:6, and 1:8, the form and the period of Rabi oscillation for spin-up electrons are the same. As discussed earlier in both linear setups, the combination with higher-order harmonics as counterpropagating laser beams only changes the amplitude of the Rabi oscillation. By comparing nine-, seven-, five-, and three-photon KD effects [18], one would find that the electron has similar spin dynamics in these scatterings. In fact all processes involving an odd number of photons with zero transverse momentum for electrons $p_x = 0$ can be suitable for spin polarization of the electron beam.

Furthermore, the study of six- and eight-photon KD effects yields similar results and for better understanding we investigate the details of the six-photon KD effect. Our analytical calculation according to Table I, for the setup with a linear fundamental laser beam and circularly polarized fifth harmonic, shows that there is no term proportional to $\sigma_\pm$ in the six-photon KD effect Rabi matrix [Eq. (5)] for the electron

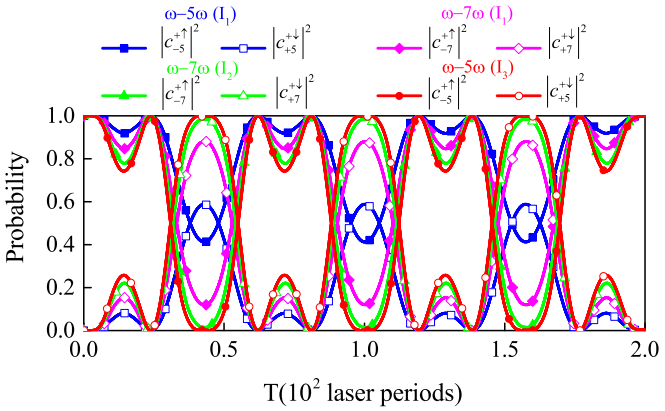

FIG. 4. Temporal evolution of the occupation probability in six- and eight-photon KD effects with linear fundamental beam and circular high-order-harmonic wave. The initial electron momentum is along the laser field direction. The numeric results are obtained with $\vec{A} = A_1 \cos(kz)\cos(\omega t)\vec{e}_x + \frac{A_2}{\sqrt{2}}\cos(nkz)\cos(n\omega t)\vec{e}_x - \frac{A_2}{\sqrt{2}}\sin(nkz)\cos(n\omega t)\vec{e}_y$ as the vector potential. The Rabi oscillations for bichromatic $(\omega : 5\omega)$ and $(\omega : 7\omega)$ standing waves with I_1 intensity show that scattering with different frequency ratio and equal intensity has the same spin dynamics. Also the Rabi oscillations for bichromatic $\omega : 5\omega$ with I_1 and I_3 and $\omega : 7\omega$ with I_1 and I_2 confirm that with changing laser amplitude, not only the electron spin dynamic in even photons involving scattering, but also the frequency of Rabi oscillations do not change. The overall intensity is in the order of $I_1 < I_2 < I_3$.

with zero transverse momentum, $p_x = 0$. By performing this setup in numerical simulation, as shown with blue (square symbol) and red (circle symbol) lines in Fig. 4, when the electron initially is in $|-5, +\uparrow\rangle$, the Rabi oscillation takes place with the $|+5, +\downarrow\rangle$ state. The symmetric spin flipping occurs and the same Rabi oscillation happens when the electron initially is spin down. The similar spin dynamic happens in the eight-photon KD effect. In Fig. 4, we compared both six- and eight-photon KD effects to investigate frequency ratios and laser amplitudes in electron spin dynamics. As it is clear, one can conclude that, with the change in laser amplitudes and, as a result, the change in the total intensity of the superposition of the two counterpropagating waves, the amplitude of the Rabi oscillation varies but the frequency of the Rabi oscillation remains constant. It is remarkable to note that although laser amplitudes change, the Rabi frequency stays constant in Fig. 4 for hybrid polarization of laser beams, similar to what is seen in Figs. 1 and 2 for linear polarization. We also concluded that by choosing the appropriate laser amplitudes, the eight-photon KD effect with higher-frequency beam could have the smaller amplitude of the Rabi oscillation. To illustrate other points of the study, we choose the six-photon KD effect for which the Rabi amplitude is fully developed, the red (circle symbol) lines in Fig. 4.

For the same combination of polarization, linear fundamental laser beam, and circularly polarized fifth harmonic, when an electron has a p_x momentum component within the polarization plane, the spin-dependent and spin-preserving scattering happens. The results are shown in Fig. 5. For the electron with initial momentum $p_z = -5k$ and $p_x = 5k$ in the

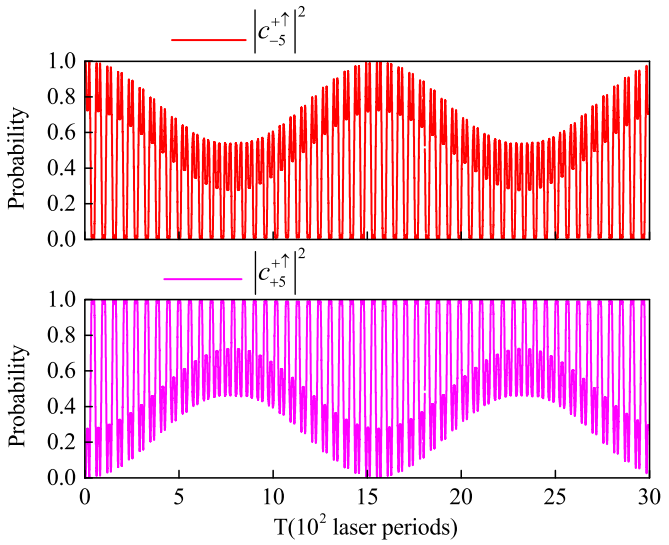

FIG. 5. Temporal evolution of the occupation probability in the six-photon KD effect with linear fundamental beam and circular fifth harmonic wave. The vector potential used for the simulation is $\vec{A} = A_1 \cos(kz)\cos(\omega t)\vec{e}_x + \frac{A_2}{\sqrt{2}}\cos(5kz)\cos(5\omega t)\vec{e}_x - \frac{A_2}{\sqrt{2}}\sin(5kz)\cos(5\omega t)\vec{e}_y$. The field parameters for beams ω and 5ω are $eA_1 = 10 \times 10^4$ eV and $eA_2 = 2 \times 10^4$ eV, respectively, with wavelength $\lambda = 0.6$ nm [the same as the red (circle symbol) lines in Fig. 4], except by choosing $p_x = 5\hbar k$ the influence of $\vec{p} \cdot \vec{A}$ is considered here. A Rabi oscillation with spin preserving can be seen, if the initial state was spin up. The probability starting from $|-5, +\downarrow\rangle$ is distributed through $|+5, +\downarrow\rangle$, $|+5, +\uparrow\rangle$, and $|-5, +\uparrow\rangle$.

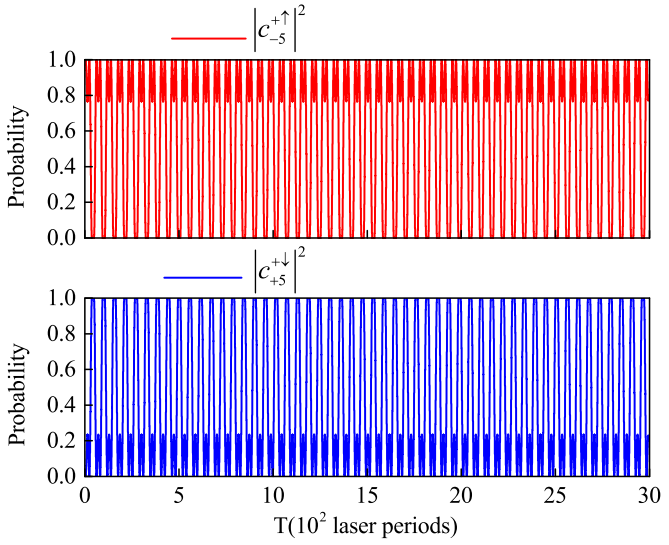

FIG. 6. Temporal evolution of the occupation probability in the six-photon KD effect with linear fundamental beam and circular fifth harmonic wave. The vector potential used for the simulation is $\vec{A} = A_1 \cos(kz)\cos(\omega t)\vec{e}_x + \frac{A_2}{\sqrt{2}}\cos(5kz)\cos(5\omega t)\vec{e}_x - \frac{A_2}{\sqrt{2}}\sin(5kz)\cos(5\omega t)\vec{e}_y$. The parameters are the same as the red (circle symbol) lines in Fig. 4 with zero transverse momentum $p_x = 0$ but for longer periods the same as in Fig. 5 for comparison.

spin-up state, a Rabi oscillation with the momentum electron $p_z = +5k$ with spin up appears. When the electron is initially in the state $|-5, +\uparrow\rangle$, no spin-flipping transition was found in our simulations. In contrast, the probability starting from $|-5, +\downarrow\rangle$ is distributed through $|+5, +\downarrow\rangle$, $|+5, +\uparrow\rangle$, and $|-5, +\uparrow\rangle$. In Fig. 5, the interaction time is considered longer, so a full period of the Rabi oscillation for exchanging modes is provided. The Rabi oscillation pattern in Fig. 5 consists of two oscillation modes: fast and slow oscillations. The fast oscillation is similar to the Rabi oscillation clearly shown in the previous figures. On the other hand, the fast oscillation is modulated by the slow oscillation. To compare the electron with or without transverse momentum p_x, see Figs. 5 and 6. Figure 6 is the exact Rabi oscillation with red (circle symbol) lines in Fig. 4 with the same conditions, but with longer interaction time. Compared to Fig. 5, only the fast oscillation mode occurs in Fig. 6. The spin effects of electrons for various polarization of laser beams in the six-photon KD effect are similar to the spin effects in the four-photon KD effect [18]. In processes involving an even number of photons with zero transverse electron momentum, the symmetry of spin flipping is observed.

IV. CONCLUSION

In this study we investigated the effect of the field polarization and the amplitudes of laser beams on the electron spin in two standing waves, when one of the standing waves has the fundamental harmonic frequency and the other has its fourth-, fifth-, sixth-, seventh-, or eighth harmonic. By increasing the frequency of counterpropagating laser beams in the multiphoton scattering, the total intensity of both laser beams increases; however, the spin behavior of the electron is not disturbed and the Rabi oscillations maintain a special behavior. Also the period and the form of the Rabi oscillation with two specific peaks remain unchanged.

The spin dependence of the Rabi matrix of these high-photon KD effects was obtained and exemplified for several polarization combinations. Comparing multiphoton scattering, three-, four-, five-, six-, seven-, and eight-photon Kapitza-Dirac effects show that the processes with odd and even numbers of photons have different effects on the electron spin dynamic. The results of analytical calculations and numerical simulations confirm that the bichromatic KD effect with an odd number of photons with circular polarization for high-order-harmonic fields acts like a spin filter. So, by properly choosing the polarization setup in the three-, five-, seven-, and nine-photon KD effects and with zero transverse momentum for the initial electron beam, the output beam can be spin polarized. The bichromatic KD effect with an even number of photons involved ($L + N$ is an even number) can scatter the electron via symmetric spin flipping. Only by controlling the polarization state of the two pulses, namely, using a suitable combination of linearly and circularly polarized light and nonzero electron momentum along laser polarization, the electron can maintain its initial spin state.

The possibility of producing spin-polarized electrons with ultraintense lasers paves the way for new applications. Polarized electrons are fundamental for the study of particle physics and are used in spin-polarized electron spectroscopy.

APPENDIX: *S*-MATRIX APPROACH FOR FIVE- AND SIX-PHOTON KAPITZA-DIRAC EFFECT

Here we describe in detail the derivation of the Rabi frequency in Eqs. (4) and (5). Our approach is based on the relativistic Volkov states which are a known solution to the Dirac equation in the presence of a plane-wave laser field. The calculation of the S matrix is the same as that used in the three-photon Kapitza-Dirac effect, except that there is a further photon that participates in the interaction [17,18]. We express the vector potential as a plane wave in radiation gauge $A_1(k_1x) = A_1(x)$, with a complex polarization 4-vector $\epsilon_1 = (0, \vec{\epsilon})$ and the wave 4-vector $k_1 = \frac{\omega}{c}(1, \vec{e}_z)$ satisfying $\epsilon_1^* \epsilon_1 = -1$ and $\epsilon_1 k_1 = 0$. A similar notation is employed for the counterpropagating wave $A_2(x)$ with ϵ_2 and $k_2 = 4k = 4k_1$ for the five-photon Kapitza-Dirac effect and $k_2 = 5k = 5k_1$ for the six-photon Kapitza-Dirac effect, respectively.

In the presence of a fourth harmonic, the S matrix for transition from $p = (p^0, p_x, 0, -4\hbar k)$ to $p' = (p^0, p_x, 0, +4\hbar k)$ by absorbing four photons from A_1 as a beam with fundamental frequency and emitting one photon into A_2 as a beam with 4ω frequency is given by

$$
\begin{aligned}
S_{\omega:4\omega} \approx \frac{ie}{\hbar cV} \int d^4x\, \bar{u}_{p',s'} \Bigg(& \not{A}_2^{(+)} \tilde{J}_4 e^{i(p'-p-4k_1)\cdot x} \\
& - \frac{e}{2c} \left[\frac{\not{A}_1^{(-)} \not{k}_1 \not{A}_2^{(+)}}{k_1 p'} + \frac{\not{A}_2^{(+)} \not{k}_1 \not{A}_1^{(-)}}{k_1 p} \right] \tilde{J}_3 e^{i(p'-p-3k_1)\cdot x} \\
& + \frac{e^2}{4c^2} \left[\frac{\not{A}_1^{(-)} \not{k}_1 \not{A}_2^{(+)} \not{k}_1 \not{A}_1^{(-)}}{(k_1 p')(k_1 p)} \right] \tilde{J}_2 e^{i(p'-p-2k_1)\cdot x} \Bigg) u_{p,s} \\
\approx \frac{ie}{2\hbar} T \bar{u}_{p',s'} & \left[a_2 \tilde{J}_4 \not{\epsilon}_2 - \frac{e a_1 a_2}{4c} \tilde{J}_3 \left(\frac{\not{\epsilon}_1 \not{k}_1 \not{\bar{\epsilon}}_2}{k_1 p'} + \frac{\not{\bar{\epsilon}}_2 \not{k}_1 \not{\epsilon}_1}{k_1 p} \right) \right] u_{p,s}.
\end{aligned}
\tag{A1}
$$

Here, $\not{A}_1^{(-)} = \frac{1}{2} a_1 \not{\epsilon}_1 e^{-ik_1 x}$ is the component that defines the absorption of one photon from A_1 with $\not{\epsilon}_1 = \epsilon_1 \gamma$, and $\not{A}_2^{(+)} = \frac{1}{2} a_2 \not{\bar{\epsilon}}_2 e^{ik_2 x}$ where $\not{\bar{\epsilon}}_2 = \epsilon_2^* \gamma$ is the component that describes the emission of one photon into A_2. Also $\tilde{J}_{1,2,3,4,5}$ are generalized Bessel functions. In this derivation only a resonant scattering process was considered, which fulfills the Bragg condition. Therefore, the d^4x integration results in the factor cVT, where T is the interaction time and V is the quantification volume [17]. Moreover, the last part of Eq. (A1) is zero and thereby it is not included in the following calculations.

The initial and scattered electron momenta for six photons are set respectively to $p = (p^0, p_x, 0, -5\hbar k)$ and $p' = (p^0, p_x, 0, +5\hbar k)$. Thus, the S matrix in Eq. (1) reads

$$
\begin{aligned}
S_{\omega:5\omega} \approx \frac{ie}{\hbar cV} \int d^4x\, \bar{u}_{p',s'} \Bigg(& \not{A}_2^{(+)} \tilde{J}_5 e^{i(p'-p-5k_1)x} \\
& - \frac{e}{2c} \left[\frac{\not{A}_1^{(-)} \not{k}_1 \not{A}_2^{(+)}}{k_1 p'} + \frac{\not{A}_2^{(+)} \not{k}_1 \not{A}_1^{(-)}}{k_1 p} \right] \tilde{J}_4 e^{i(p'-p-4k_1)x} \\
& + \frac{e^2}{4c^2} \left[\frac{\not{A}_1^{(-)} \not{k}_1 \not{A}_2^{(+)} \not{k}_1 \not{A}_1^{(-)}}{(k_1 p')(k_1 p)} \right] \tilde{J}_3 e^{i(p'-p-3k_1)x} \Bigg) u_{p,s} \\
\approx \frac{ie}{2\hbar} T \bar{u}_{p',s'} & \left[a_2 \tilde{J}_5 \not{\epsilon}_2 - \frac{e a_1 a_2}{4c} \tilde{J}_4 \left(\frac{\not{\epsilon}_1 \not{k}_1 \not{\bar{\epsilon}}_2}{k_1 p'} + \frac{\not{\bar{\epsilon}}_2 \not{k}_1 \not{\epsilon}_1}{k_1 p} \right) \right] u_{p,s}.
\end{aligned}
\tag{A2}
$$

The Dirac spinors mentioned above in Eqs. (A1) and (A2) are constructed from the corresponding Pauli spinors χ_s through

$$u_{(p,s)} = \frac{1}{\sqrt{2mc(p^0+mc)}} \begin{pmatrix} (p^0+mc)\chi_s \\ \vec{p}\cdot\vec{\sigma}\,\chi_s \end{pmatrix}. \tag{A3}$$

Keeping the mentioned conditions in mind, we can calculate the first parts of Eqs. (A1) and (A2), respectively, as

$$(\bar{u}_{p',s'}\bar{\not{\epsilon}}_2 u_{p,s})_{s',s} = -\frac{p_x}{mc}\vec{\epsilon}_2^{\,*}\cdot\vec{e}_x + \frac{4i\hbar\omega}{mc^2}(\vec{\epsilon}_2^{\,*}\times\vec{e}_z)\cdot\vec{\sigma}, \tag{A4}$$

$$(\bar{u}_{p',s'}\bar{\not{\epsilon}}_2 u_{p,s})_{s',s} = -\frac{p_x}{mc}\vec{\epsilon}_2^{\,*}\cdot\vec{e}_x + \frac{5i\hbar\omega}{mc^2}(\vec{\epsilon}_2^{\,*}\times\vec{e}_z)\cdot\vec{\sigma}. \tag{A5}$$

In a similar way for the second part of Eqs. (A1) and (A2) we find respectively

$$\left(\bar{u}_{p',s'}\left[\frac{\not{\epsilon}_1\not{k}_1\bar{\not{\epsilon}}_2}{k_1p'} + \frac{\bar{\not{\epsilon}}_2\not{k}_1\not{\epsilon}_1}{k_1p}\right]u_{p,s}\right)_{s',s}$$
$$\approx \frac{2\vec{\epsilon}_1\cdot\vec{\epsilon}_2^{\,*}}{mc} - \frac{8i\hbar\omega}{m^2c^3}(\vec{\epsilon}_1\times\vec{\epsilon}_2^{\,*})\cdot\vec{\sigma}, \tag{A6}$$

$$\left(\bar{u}_{p',s'}\left[\frac{\not{\epsilon}_1\not{k}_1\bar{\not{\epsilon}}_2}{k_1p'} + \frac{\bar{\not{\epsilon}}_2\not{k}_1\not{\epsilon}_1}{k_1p}\right]u_{p,s}\right)_{s',s}$$
$$\approx \frac{2\vec{\epsilon}_1\cdot\vec{\epsilon}_2^{\,*}}{mc} - \frac{10i\hbar\omega}{m^2c^3}(\vec{\epsilon}_1\times\vec{\epsilon}_2^{\,*})\cdot\vec{\sigma}. \tag{A7}$$

Also from the Taylor series of the generalized Bessel functions, we can estimate

$$\tilde{J}_1 \approx \frac{\alpha_p-\alpha'_p}{2}, \quad \tilde{J}_2 \approx \frac{(\alpha_p-\alpha'_p)^2}{8} - \epsilon_1^2\frac{(\beta_p-\beta'_p)}{2},$$
$$\tilde{J}_3 \approx \frac{(\alpha_p-\alpha'_p)^3}{48} - \frac{(\alpha_p-\alpha'_p)}{2}\epsilon_1^2\frac{(\beta_p-\beta'_p)}{2},$$
$$\tilde{J}_4 \approx \frac{(\alpha_p-\alpha'_p)^4}{384} - \frac{(\alpha_p-\alpha'_p)^2}{8}\epsilon_1^2\frac{(\beta_p-\beta'_p)}{2} + \epsilon_1^4\frac{(\beta_p-\beta'_p)^2}{8},$$
$$\tilde{J}_5 \approx \frac{(\alpha_p-\alpha'_p)^5}{3840} - \frac{(\alpha_p-\alpha'_p)^3}{48}\epsilon_1^2\frac{(\beta_p-\beta'_p)}{2} + \frac{(\alpha_p-\alpha'_p)}{2}\epsilon_1^4\frac{(\beta_p-\beta'_p)^2}{8}. \tag{A8}$$

Considering $\alpha_p-\alpha'_p = \frac{-8ea_1p_x(\vec{\epsilon}_1\cdot\vec{e}_x)}{m^2c^3}$ and $\beta_p-\beta'_p = \frac{e^2a_1^2}{m^2c^4}$ for the bichromatic ($\omega:4\omega$) Kapitza-Dirac effect and putting all this together, the S matrix of Eq. (A1) for small transverse momentum is estimated as

$$S_{\omega:4\omega} \approx \frac{i}{2}T\frac{e^5a_1^4a_2}{m^5c^{10}}\left[\frac{-1}{8\hbar}p_xc\vec{\epsilon}_1^{\,4}(\vec{\epsilon}_2^{\,*}\cdot\vec{e}_x) - \frac{i}{\hbar}p_xc(\vec{\epsilon}_1\cdot\vec{e}_x)\vec{\epsilon}_1^{\,2}(\vec{\epsilon}_1\cdot\vec{\epsilon}_2^{\,*}) + \frac{i}{2}\omega\vec{\epsilon}_1^{\,4}(\vec{\epsilon}_2^{\,*}\times\vec{e}_z)\cdot\vec{\sigma} + \frac{4i}{mc}p_x\omega(\vec{\epsilon}_1\cdot\vec{e}_x)\vec{\epsilon}_1^{\,2}(\vec{\epsilon}_1\times\vec{\epsilon}_2^{\,*})\cdot\vec{\sigma}\right] = \frac{i}{2}T\xi_1^4\xi_2\hat{\Omega}. \tag{A9}$$

Here, $\xi_{1,2} = \frac{ea_{1,2}}{mc^2}$ are the common dimensionless field amplitudes used in atomic physics. Finally, the Rabi frequency $\Omega_{\omega:4\omega}$ leading order in m^{-1} is derived as

$$\hat{\Omega}_{\omega:4\omega} = +\frac{i}{2}\omega\vec{\epsilon}_1^{\,4}(\vec{\epsilon}_2^{\,*}\times\vec{e}_z)\cdot\vec{\sigma} - p_xc\left[\frac{1}{8}\vec{\epsilon}_1^{\,4}(\vec{\epsilon}_2^{\,*}\cdot\vec{e}_x) + i(\vec{\epsilon}_1\cdot\vec{e}_x)\vec{\epsilon}_1^{\,2}(\vec{\epsilon}_1\cdot\vec{\epsilon}_2^{\,*})\right] + 4i\frac{p_x}{c}\omega(\vec{\epsilon}_1\cdot\vec{e}_x)\vec{\epsilon}_1^{\,2}(\vec{\epsilon}_1\times\vec{\epsilon}_2^{\,*})\cdot\vec{\sigma}. \tag{A10}$$

From $\alpha_p-\alpha'_p = \frac{-10ea_1p_x(\vec{\epsilon}_1\cdot\vec{e}_x)}{m^2c^3}$ and $\beta_p-\beta'_p = \frac{10e^2a_1^2}{8m^2c^4}$ for the bichromatic ($\omega:5\omega$) Kapitza-Dirac effect in the order of m^{-1}, the matrix is

$$S_{\omega:5\omega} \approx \frac{i}{2}T\frac{e^6a_1^5a_2}{m^6c^{12}}\left[+\frac{125i}{256}\omega\vec{\epsilon}_1^{\,4}(\vec{\epsilon}_1\times\vec{\epsilon}_2^{\,*})\cdot\vec{\sigma} - \frac{625i}{128}\frac{p_x\omega}{mc}(\vec{\epsilon}_1\cdot\vec{e}_x)\vec{\epsilon}_1^{\,4}(\vec{\epsilon}_2^{\,*}\times\vec{e}_z)\cdot\vec{\sigma}\right] = \frac{i}{2}T\xi_1^5\xi_2\hat{\Omega}, \tag{A11}$$

and the final Rabi frequency of the six-photon Kapitza-Dirac effect has the form of

$$\hat{\Omega}_{\omega:5\omega} = +\frac{125i}{256}\omega\vec{\epsilon}_1^{\,4}(\vec{\epsilon}_1\times\vec{\epsilon}_2^{\,*})\cdot\vec{\sigma} - \frac{625i}{128}\frac{p_x}{c}\omega(\vec{\epsilon}_1\cdot\vec{e}_x)\vec{\epsilon}_1^{\,4}(\vec{\epsilon}_2^{\,*}\times\vec{e}_z)\cdot\vec{\sigma}. \tag{A12}$$

[1] The Vulcan facility, http://www.clf.stfc.ac.uk/Pages/The-Vulcan-10-Petawatt-Project.aspx.

[2] The Extreme Light Infrastructure (ELI), http://www.eli-laser.eu/.

[3] Exawatt Center for Extreme Light Studies (XCELS), http://www.xcels.iapras.ru/.

[4] J. Kessler, *Polarized Electrons* (Springer, Berlin, 1985).

[5] Y.-F. Li, R. Shaisultanov, K. Z. Hatsagortsyan, F. Wan, C. H. Keitel, and J.-X. Li, Phys. Rev. Lett. **122**, 154801 (2019).

[6] Y.-Y. Chen, P.-L. He, R. Shaisultanov, K. Z. Hatsagortsyan, and C. H. Keitel, Phys. Rev. Lett. **123**, 174801 (2019).

[7] M. Wen, M. Tamburini, and C. H. Keitel, Phys. Rev. Lett. **122**, 214801 (2019).

[8] D. Del Sorbo, D. Seipt, T. G. Blackburn, A. G. R. Thomas, C. D. Murphy, J. G. Kirk, and C. P. Ridgers, Phys. Rev. A **96**, 043407 (2017).

[9] D. Seipt, D. Del Sorbo, C. P. Ridgers, and A. G. R. Thomas, arXiv:1904.12037.

[10] M. M. Dellweg and C. Müller, Phys. Rev. Lett. **118**, 070403 (2017).

[11] P. L. Kapitza and P. A. Dirac, Math. Proc. Cambridge Philos. Soc. **29**, 279 (1933).

[12] S. Ahrens, H. Bauke, C. H. Keitel, and C. Muller, Phys. Rev. Lett. **109**, 043601 (2012).

[13] S. Ahrens, H. Bauke, C. H. Keitel, and C. Müller, Phys. Rev. A **88**, 012115 (2013).

[14] M. M. Dellweg and C. Müller, Phys. Rev. A **91**, 062102 (2015).
[15] M. M. Dellweg, H. M. Awwad, and C. Müller, Phys. Rev. A **94**, 022122 (2016).
[16] S. Ahrens, Phys. Rev. A **96**, 052132 (2017).
[17] M. M. Dellweg and C. Müller, Phys. Rev. A **95**, 042124 (2017).
[18] A. Ebadati, M. Vafaee, and B. Shokri, Phys. Rev. A **98**, 032505 (2018).
[19] M. Kozák, N. Schönenberger, and P. Hommelhoff, Phys. Rev. Lett. **120**, 103203 (2018).
[20] M. Kozák, T. Eckstein, N. Schönenberger, and P. Hommelhoff, Nat. Phys. **14**, 121 (2018).
[21] M. Kozák, Phys. Rev. A **98**, 013407 (2018).
[22] D. M. Volkov, Z. Phys. **94**, 250 (1935).
[23] V. I. Ritus, J. Russ. Laser Res. **6**, 497 (1985).
[24] P. Panek, J. Z. Kaminski, and F. Ehlotzky, Phys. Rev. A **65**, 022712 (2002).
[25] For current information, see http://www.xfel.eu and https://lcls.slac.stanford.edu.